Real-Time, Non-Contacting Position Tracking of Medical Devices and Surgical Tools through the Analysis of Magnetic Field Vectors

Mohammad Odeh[1]
Edward D. Nichols[1]
Fluvio L. Lobo Fenoglietto[1]
Jack B. Stubbs[1]

Institute for Simulation and Training, Center for Applied Research, University of Central Florida[1]

1 Background

As the demand for increasingly advanced invasive medical procedures rises with the average age of the population, it also becomes increasingly compelling to facilitate and extend the spatial awareness and dexterity of surgeons, both human and robotic. One may accomplish this by tracking an object digitally and representing its form and motion in a close virtual model of the area of interest within the patient, such as through an augmented reality platform. Several groups across a diverse range of academia and industry have competed to develop marginal improvements to methods of digitally tracking objects [1, 3, 5, and 6]. In the entertainment industry in particular, object tracking is a fundamental way of bringing life-like motion to an object represented in virtual space. The generally accepted approach is to use expansive, multi-camera computer vision (CV) systems to yield real-time tracking [4]. However, this approach is not suited for medical applications; CV is limited by a strict field of view. Accurately tracking surgical instruments inside of organic tissues must then be done another way.

Of the methods presently being investigated, none are as applicable in a medical context as magnetic field sensing. Human tissues are permeable to magnetic flux, and magnetic fields are well characterized. Upon this motivation, we have constructed an inexpensive device from off-the-shelf parts that enables the tracking of a permanent magnet on a surface to serve as a foundation for future work in this field.

2 Methods

2.1 Analytical Foundation

Electromagnetic fields are characterized by fundamental principles. Given a classic magnetic dipole centered at the origin, its magnetic induction can be expressed as:

$$\vec{\mathbf{B}} = \frac{\mu_0}{4\pi} * \frac{3\hat{\mathbf{r}}(\vec{\boldsymbol{\mu}} \bullet \hat{\mathbf{r}}) - \vec{\boldsymbol{\mu}}}{\mathrm{r}^3} \quad (1)$$

Whereby the relationship is dependent on the orientation and strength of its magnetic moment vector, given by $\vec{\boldsymbol{\mu}}$, as well as the location of the arbitrary point of interest with respect to the center of the magnet, represented by vector $\vec{\mathbf{r}}$. Equation (1) can be modified to express the strength of the magnetic field $\vec{\mathbf{H}}$, which is what an observing magnetometer normal to the level surface of the magnetic field would perceive; which may further be broken into a more convenient polar component form, given the intrinsic rotational symmetry of isofield lines about $\vec{\boldsymbol{\mu}}$.

Based on the work of Chen *et al* [5], expressing the location of the center of a magnet with respect to the magnetic field vectors observed by three sensors in predefined relative positions fully satisfies a system of equations when the magnet is in a fixed North pole orientation along the system's internally defined x-axis:

$$\left\|\vec{\mathbf{H}_i}\right\| = \sqrt{\frac{\mathrm{K}(3\cos^2\theta_i + 1)}{{r_i}^6}} \quad (2)$$

$$\|\vec{\mathbf{r}_i}\| = [(\mathrm{x} + \Delta x_i)^2 + (\mathrm{y} + \Delta y_i)^2 + (\mathrm{z} + z_i)^2] \quad (3)$$

$$\cos\theta_i = \frac{z}{r_i} \quad (4)$$

Whereby, i represents a sensor in the array, $\|\vec{\mathbf{r}_i}\| = r$ is the distance to the center of the magnet for the sensor, Δ_i is the relative offset from a designated origin with respect to the sensor, θ_i represents the angle made by the north pole of the magnet and the radial component of $\vec{\mathbf{H}}$, and K represents a constant that encompasses the magnitude of the dipole moment, magnetic permeability of free space μ_0, and the relative permeability of the magnet's own material.

However, one must maintain certain minimum assumptions for a solution to converge numerically.

1. An origin must be defined with respect to the relative fixed positions and orientations of the sensors.
2. The constant value of the magnetic field strength coefficient K of an arbitrary magnet has been closely approximated, or is otherwise known.
3. A constant magnetic field source of perceivable threshold exists within range of at least three sensors in the sensor array.

In addition, to refine accuracy, certain physical restrictions facilitate these conditions.

1. Ambient magnetic fields must be mitigated; or the signal must be otherwise overcome.
2. The magnet's form factor is minimized to yield closer adherence to presupposed principles.

To begin achieving these conditions, we designated the sensor in the bottom left corner of our 2D sensor array (Figure 1) to be the origin. All sensors' axis in the array are aligned with each other.

2.2 Magnet Selection

While the work of Chen *et al.* [6] has demonstrated feasibility of multiple object tracking using electromagnets, our team decided to pursue an approach that would require the least number of modifications to the device, tool, or end-effector to be tracked. Hence, permanent magnets were chosen to test our

approach. Both magnets were assumed to have an ideal magnetic dipole field. The magnitude of each magnet's dipole moment K was calculated empirically (Table 1).

2.3 Empirical Approximation of K

Our team devised an empirical approach to approximate the value of K using a single *SparkFun LSM9DS1 IMU* and a custom CNC machine. Three out of the nine degrees of freedom (DoF) from the *LSM9DS1 IMU* are given by a magnetometer, used here measure the strength of the magnetic field $\vec{\mathbf{H}}$ generated by the permanent magnet in question. The CNC was then used to move the permanent magnet precisely, along a single axis (x axis), towards the magnetometer, thus simplifying Eqns. (2), (3) and (4) into Equation (5).

$$\mathrm{K} = \left\|\vec{\mathbf{H}}\right\|^{\mathbf{2}} x^2 \tag{5}$$

The protocol for the approximation of K, for each magnet, can be summarized in the following six steps:

1. The magnet was placed at a distance of 50mm away from the IMU sensor such that it reads (H_x, H_y, H_z) and $(x = 50mm, y \cong 0, z \cong 0)$.
2. A value for $\left\|\vec{\mathbf{H}_i}\right\|$ was obtained and an accurate approximation for K was computed using Eqn. (5).
3. The magnet was moved Δx=10mm to $(x + \Delta x, y \cong 0, z \cong 0)$.
4. Another sample of K was approximated from a new $\left\|\vec{\mathbf{H}_i}\right\|$.
5. Steps 3 and 4 were repeated up to x =75mm, recording the values of x, $\left\|\vec{\mathbf{H}_i}\right\|$ and K each time.
6. An approximated result of K was yielded from averaging the sampled points.

It is worth noting that the value of K might vary along the different x positions, nonetheless, such differences are minute and can be attributed to the background magnetic fields overshadowing that of the magnets'. In addition, it is possible to further improve the accuracy of the approximated value of K by minimizing H_y and H_z components of the magnetic field readings. However, that requires further manipulation of the positioning of the magnets such that the magnet is moved in a step-wise fashion along the $x, y,$ and z axes until the condition of $H_y \cong 0$ and $H_z \cong 0$ is satisfied and then using Eqns. (2), (3), and (4) to approximate the value of K. As long as both $H_y, H_z \leq 1.0 \times 10^{-2}$ the approximated value of K yielded physically reasonable position solutions. Nevertheless, the gain in accuracy using such an arduous method was not significant and the team opted to use the protocol defined earlier to approximate the value of K for any future work.

2.4 2D Sensor Array

Having calculated K, our team proceeded to build a set-up capable of tracking either magnet. While only three magnetometers were required to derive the position of the magnets, an array of six *SparkFun LSM9DS1 IMU* was built to enclose a tracking area and extend the tracking capabilities of the system. Due to I^2C address conflicts, magnetometer communication was mediated using a *SparkFun 74HC4051 8-channel multiplexer*. Data was driven through an Arduino-compatible microcontroller such as the *Arduino Mega 2560* or *PJRC's Teensy 3.2* (Figure 1). Microcontrollers formatted and transmitted magnetometer data through a Serial Bus to a PC running a custom Python script. The entire set-up was mounted over a metric optics breadboard with M6 taps every 25 mm. 3D printed holders were fabricated to secure the magnetometers and permanent magnets. 3D printing was also used to create guides for motion tracking experiments (Figure 1).

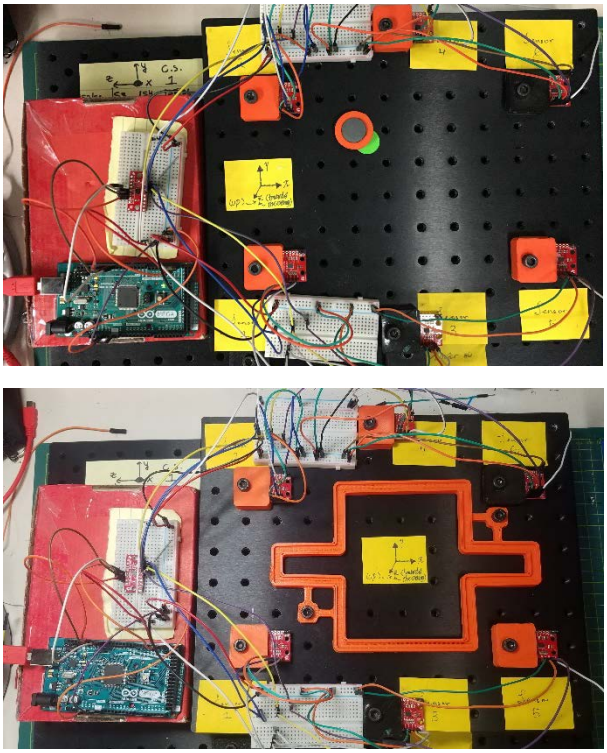

Figure 1: 2D, 6-Magnetometer Sensor Array determining position accuracy (top) and motion tracking using a 3D-printed guide (bottom)

Sensor readings were taken by the magnetometers at 80Hz, yielding the XYZ components of $\vec{\mathbf{H}}$ with respect to the sensor orientation. Geomagnetism was partially accounted for using the board's built-in declination adjustment function. To mitigate the effect of remaining ambient magnetic fields, sensor readings were averaged over 50 readings, for each sensor, upon reset and the respective result was subtracted from later readings. Drifting was observed to be minimal, yet further mitigation was left as future work. Readings henceforth started at ±20 Milligauss and ranged to ±16 Gauss, according to the built-in 16-bit analog to digital converter in the chip.

2.3 Position Tracking Algorithm

Data retrieval and position tracking was driven by a custom Python script developed on a PC. Based on Eqns. (2), (3) and (4), each magnetometer allowed the Python script to assemble one equation, for a total of six equations using the entire array. The resulting non-linear system had no analytical solution, thus requiring a numerical approach. SciPy's implementation of the Levenberg-Marquardt (LMA) method was used to solve the

resulting non-linear system. Given that SciPy's LMA lacked support for over-constrained systems, three of the six magnetometer were ignored on every iteration. The script constructed the system of equations using the data from the three magnetometers with the largest $\|\vec{\mathbf{H}}\|$.

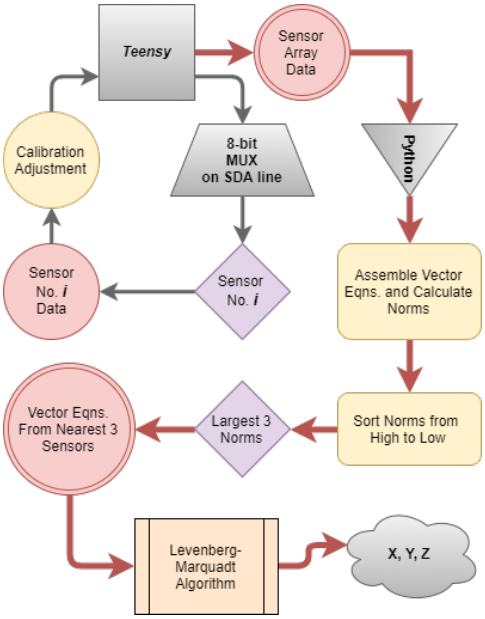

Figure 2: Overall System and Position Tracking Algorithm Flowchart

The LMA was chosen for its robustness and speed of convergence. SciPy's LMA combines Newton-Raphson's algorithm and the Steepest Descent method to converge even in the case of a poor initial guess. However, like any numerical method, effective convergence still relies on the initial guess' proximity to the solution. To overcome this issue, the centroid of the triangle described by the three magnetometers with the largest readings was used as the initial guess.

Upon convergence of the LMA, values were logged to determine point accuracy (Table 2, 3) and motion tracking capabilities (Figure 3, 4). The entire process described above, from sensor calibration to data collection and numerical solution has been summarized in Figure 2.

3 Results

3.1 Approximation of K

Following the CNC-based approximation protocol described earlier, the magnitude of the magnetic field moment K was determined for two permanent magnets (Table 1).

Table 1. Permanent Magnet Information

Magnet	Diameter (mm)	K (G2m6)
Small	18	7.27E-08
Large	30	0.000001092

3.2 Point Accuracy

Using our 2D sensor array, position tracking accuracy was studied by placing each permanent magnet in 20 different locations within the array. On average, 20 seconds of sensor readings were recorded for each location. The difference between the expected and observed X and Y positions was recorded, in millimeters, as X_{off} and Y_{off}. A percentage error was calculated as the ratio of these differences to the original X and Y positions. The values reported here represent the average position difference and error among the 20 points sampled using each magnet (Table 2, 3).

Table 2. Point Accuracy Results for Large Magnet

Statistics	X_{off} (mm)	Y_{off} (mm)	X_{off} % Error	Y_{off} % Error
Mean	0.6744	0.9654	0.0074	0.0244
Standard Error	0.0861	0.2149	0.0012	0.0059
Standard Deviation	0.3849	0.9612	0.0054	0.0264
Range	1.3146	3.6753	0.0223	0.0883
Minimum	0.0055	0.0116	0.0001	0.0001
Maximum	1.3201	3.6869	0.0224	0.0885
Count	20	20	20	20

Table 3. Point Accuracy Results for Small Magnet

Statistics	X_{off} (mm)	Y_{off} (mm)	X_{off} % Error	Y_{off} % Error
Mean	1.2368	1.4819	0.0156	0.0354
Standard Error	0.2689	0.2196	0.0048	0.0093
Standard Deviation	1.2024	0.9819	0.0214	0.0416
Range	4.3165	3.2383	0.0863	0.1327
Minimum	0.0097	0.1563	0.0002	0.0031
Maximum	4.3262	3.3946	0.0865	0.1358
Count	20	20	20	20

The position difference and thus the error was observed to be greater in the case of the small permanent magnet. The weaker magnetic field and magnetic field moment K can support this observation.

3.1 Motion Tracking

In addition to single point accuracy, our system was tested for motion tracking. 3D-printed tracks were printed to guide the magnets on a constrained path as its position was approximated by the sensor array (Figure 1). Two tracks were designed (squared and curved), printed and tested using the two permanent magnets. Scatter plots were generated from each experiment (Figure 3, 4).

Motion tracking experiments revealed areas of future work for our team. Scatters revealed some position inaccuracies that could be accounted for by considering the motion was not smooth (the magnet was moved along the track by hand). Furthermore, some inaccuracies could also be irrelevant when considering the actual size of the permanent magnet. Two dashed lines, following the color pattern used for the scatter, represent the approximate size of each magnet (Figure 3, 4). Overall position inaccuracies can be inferred by looking at the corresponding track designs (depicted on the top-right corner of each graph). Additionally, each track required a few minutes for completion (data gathering and plotting) which will lead our team to study hardware and software bottlenecks in pursuit of more rapid tracking.

Note that the coordinate system defined by mathematical principles is executed within our LMA algorithm; wherein a cylindrical magnet, orienting its North Pole along the LMA's X-axis, lays normal to the surface. Yet, our printed output reflects a more convenient representation of the Euclidean space, whereby the LMA coordinate system is rotated about the Y-axis by 90° to yield the common orientation (whereby the X'-axis extends to the right, as in Figure 3 and 4).

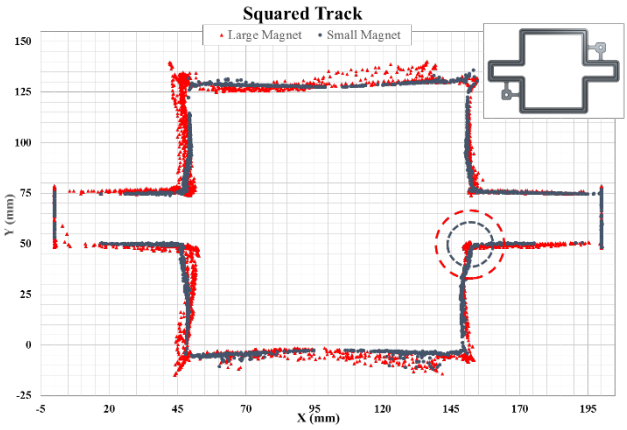

Figure 3: Motion tracking of small and large magnet along squared track.

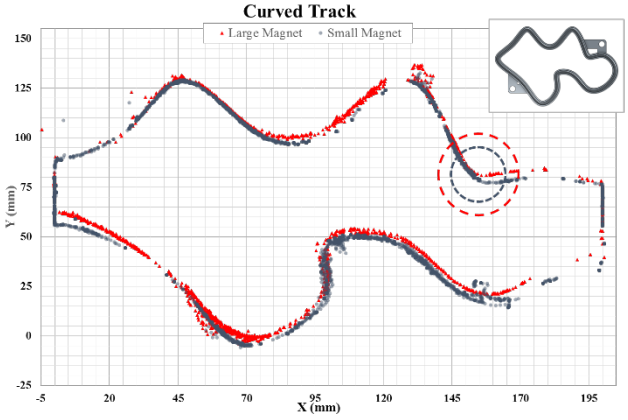

Figure 4: Motion tracking of small and large magnet along curved track.

4 Interpretation and Future Work

The most significant accomplishments of the work presented here encompass the design and implementation of a non-contacting position tracking method and system using affordable, open-source hardware and software components. The system gave accurate position results and performed over a wider range than other applications [2, 5, and 6]. Furthermore, our method worked for two off-the-shelf permanent magnets. This capability allows for easy adaptation to devices or applications where after-market modifications must be kept to a minimum. In particular, using current-driven electromagnets. Finally, our team developed an algorithm capable of approximating initial guesses in order to improve speed of convergence.

Throughout the development of our system, our team encountered some limitations which had an effect on the results presented here. Hence, further optimization is required, especially and including, a more robust mitigation of ambient fields and maximized throughput rate (which is heavily dependent on computation time). Finally, a thorough characterization of the system's performance in 3D space, especially at random orientations of the magnet, must still be done.

Moving forward we intend to improve upon the system, by optimizing the execution of LMA with better initial guesses and smoother data inputs; enable the approximation of a magnet's orientation, by tracking the path of the magnet and the sensor array's magnetic field vector components across time; increasing the measurement accuracy, by refining approximations of K; miniaturizing the device to a more convenient form, **to better suit our application**; and moving to more complex multi-pole objects, such as combinations of magnets; and building a 3D visualization of system output in real-time.

References

[1] Han, X., Seki, H., Kamiya, Y., and Hikizu, M. "Wearable handwriting input device using magnetic field Geomagnetism cancellation in position calculation." *Precision Engineering* Vol. 33 Issue 1 (2009), pp: 37-43. DOI 10.1016/j.precisioneng.2008.03.008.

[2] Han, X., Seki, H., Kamiya, Y., and Hikizu, M. "Wearable handwriting input device using magnetic field 2nd report: Influence of misalignment of magnet and writing plane." *Precision Engineering* Vol. 34 Issue 3 (2010), pp: 425-430. DOI 10.1016/j.precisioneng.2009.12.005

[3] Raab, F., Blood, E., Steiner, T., and Jones, H. "Magnetic Position and Orientation Tracking System" *IEEE Transactions on Aerospace and Electronic Systems* Vol. AES-15 No. 5 (1979), pp: 709-718

[4] Moeslund, T., and Granum, E. "A Survey of Computer Vision-Based Human Motion Capture." *Computer Vision and Image Understanding* Vol. 81, Issue 3 (2001), pp: 231-268. DOI 10.1006/cviu.2000.0897

[5] Chen, K., Lyons, K., White, S., and Patel, S. "uTrack: 3D Input Using Two Magnetic Sensors" In *Proceedings of the 26th Annual ACM Symposium on User Interface Software and Technology (UIST 2013).* pp: 237-244. St. Andrews, UK, October 8th-11th, 2013. DOI 10.1145/2501988.2502035

[6] Chen, K., Patel, S., and Keller, S. "Finexus: Tracking Precise Motions of Multiple Fingertips Using Magnetic Sensing" In *Proceedings of the 2016 CHI Conference on Human Factors in Computing Systems (CHI 2016), ACM.* pp: 1504-1514. San Jose, California, USA, May 7th-12th, 2016. DOI 10.1145/2858036.2858125

[7] Yoon, S., Huo, K., and Ramani, K. "TMotion: Embedded 3D Mobile Input using Magnetic Sensing Technique" In *Proceedings of the Tenth International Conference on Tangible, Embedded, and Embodied Interaction (TEI 2016), ACM.* pp: 21-29. Eindhoven, Netherlands, February 14th-17th, 2016. DOI 10.1145/2839462.2839463